

High-throughput computational screening for bipolar magnetic semiconductors

Haidi Wang¹, Qingqing Feng², Xingxing Li^{2*} & Jinlong Yang^{2*}

¹*School of Physics, Hefei University of Technology, Hefei, Anhui 230601, China*

²*Hefei National Laboratory for Physical Sciences at Microscale, Department of Chemical Physics, and Synergetic Innovation Center of Quantum Information and Quantum Physics, University of Science and Technology of China, Hefei, Anhui 230026, China*

Correspondence Xingxing Li (lix@ustc.edu.cn) & Jinlong Yang (jlyang@ustc.edu.cn)

Searching ferromagnetic semiconductor materials with electrically controllable spin polarization is a long-term challenge for spintronics. Bipolar magnetic semiconductors (BMS), with valence and conduction band edges fully spin-polarized in different spin directions, show great promise in this aspect because the carrier's spin polarization direction can be easily tuned by voltage gate. Here, we propose a standard high-throughput computational screening scheme for searching BMS materials. The application of this scheme to the Materials Project database gives 11 intrinsic BMS materials (1 experimental and 10 theoretical) from nearly ~ 40000 structures. Among them, a room temperature BMS $\text{Li}_2\text{V}_3\text{TeO}_8$ (mp-771246) is discovered with a Curie temperature of 478 K. Moreover, the BMS feature can be maintained well when cutting the bulk $\text{Li}_2\text{V}_3\text{TeO}_8$ into (001) nanofilms for realistic applica-

tions. This work provides a feasible solution for discovering novel intrinsic BMS materials from various crystal structure databases, paving the way for realizing electric-field controlled spintronic devices.

Introduction

In the era of big data, information transmission, processing and storage are under spotlight in the research field. The development and utilization of the freedom of spin of electrons in this new era is the epitome of the so-called spintronics.¹⁻⁴ Its outstanding features, such as faster data processing speed, higher circuit integration, lower energy consumption, and non-volatility, making it particularly advantageous in information transmission and storage.⁵ As a foundation of spintronics, functional spintronics materials such as half metallic ferromagnets (HMF), half semiconductors (HSC) and spin gapless semiconductors (SGS) have been widely investigated.⁶⁻⁹ At the same time, we have previously proposed a new conceptual material, namely, bipolar magnetic semiconductor (BMS),¹⁰ which is considered to be a promising spintronics material with tunable feature. Specifically, thanks to its special band structure, the current passing through this kind of material can be totally spin polarized on the one hand, and the spin polarization direction of the current can be directly tuned by simply applying gate voltage on the other hand.

Considering that BMS is deemed as an ideal material for electric control of spin polarization, it has become a hot spot in the field of physical chemistry in recent years. Although BMS has broad application prospects and some BMS materials have been proposed,¹¹⁻¹⁸ there is still a long way to go from theoretical study to experiment implementation. The primary obstacle is that the existing

BMS materials are problematic in reality in the following aspects: 1) most theoretically designed BMS materials are extrinsic,^{19,20} i.e. based on chemical or physical modifications, which makes the experimental synthesizing difficult 2) magnetic orders are only stable at very low temperatures,²¹ making it unfeasible for room temperature devices. In addition, the experimental available BMS candidates are far from sufficient on account of the low efficiency of traditional trial and error method. Therefore, it is necessary to unveil more potential BMS materials with the help of new technical means, thereby paving the way for the synthesis and application of spintronic devices.

In recent years, with the proposal of the "Material Genome Project",^{22,23} high-throughput screening technology has been widely used in the field of material design, and a series of important research results have been achieved. For example, Ceder et al.²⁴ successfully predicted one high-energy density lithium battery material $\text{LiCo}_{0.5}\text{Zr}_{0.5}\text{O}_2$ through high-throughput screening within the $\text{LiAl}_{0.5}\text{B}_{0.5}\text{O}_2$ compound structure space, which has been proved by experiments; Yan et al.,²⁵ by integrating high-throughput theory and experimental technology, discovered 8 ternary vanadates that can be used for photocatalysis and revealed the significance of VO_4 unit in the structure. Recently, Chen et al.²⁶ screened 40,000 compounds from the Materials Project and discovered a ferromagnetic half semiconductor (In_2MnO_7) with a Curie temperature about 130 K. In view of the abundant achievements of high-throughput screening, we believe that it should also be adapted to search for BMS materials more effectively.

In this work, we propose a standard high-throughput computational screening scheme for exploring BMS materials from nowadays crystal structure databases based on six filters, i.e. ini-

tialization filter, magnetic filter, stability filter, band gap filter, doping filter and refinement filters. The validity of the proposed scheme is confirmed by its successful application to the Materials Project (MP)^{27,28} database, which contains about one hundred thousand experimentally synthesized and also theoretically predicted inorganic compounds with calculated electronic, magnetic, elastic and piezoelectric properties. After large scale computational screening, we obtain 11 candidate BMS materials for spintronics application, among which one BMS material with room temperature ferromagnetism has been predicted.

Results

As is shown in Figure 1, the high-throughput screening process of BMS materials includes two groups of descriptors: primary descriptors (up panel in Figure 1) and secondary descriptors (lower right panel in Figure 1). The primary descriptors consist of five filters, including Initialization (I) filter, magnetic (M) filter, stability (S) filter, band gap (G) filter and doping (D) filter. The function of five filters are described as follows: (1) **I filter**. This filter is used to build the repository for screening. Considering the requirements of magnetic semiconductors, we select all structures with one or more elements in the set of { V, Cr, Mn, Fe, Co, Ni}, where the metal and alloy structures are excluded. (2) **M filter**. According to band theory, one spin-polarized band has one electron. The fractional magnetic moment must have fractional occupation, which corresponds to metals. Therefore, the M filter selects the structures that only has non-zero integer magnetic moment, which, to some extent, can guarantee that the candidates are magnetic semiconductor materials. At the same time, to reduce the computational complexity, we only select the structures

with ferromagnetic (FM) order. (3) **S filter**. For stability of a compound, two important factors are considered here, including formation energy (E_f) and the energy above convex hull (E_{abh}). The formation energy²⁹ of an compound is the energy required to produce the system from the most stable crystal structures of the individual components, which is defined as

$$E_f = \frac{E(A_xB_y) - xE(A) - yE(B)}{x + y} \quad (1)$$

where $E(A_xB_y)$ is the total energy of the material A_xB_y , and $E(A)$ and $E(B)$ are the average energies of the elements A and B in their stable crystal at 0K. For E_{abh} , it measures the energy for a material to decompose into the set of the most stable materials. A positive E_{abh} indicates that this material is unstable with respect to such decomposition. A zero E_{abh} indicates that this is the most stable material at its composition.^{29,30} Generally speaking, those compounds with negative E_f are easy to be synthesized. However, considering the error of DFT calculations, we use an appropriate standard to select the candidate structures, namely, E_f less than 0.01 eV/atom. In addition, it is generally believed that structures with E_{abh} less than 0.1 eV/atom can be synthesized experimentally.^{29,30} In short, the standard for S filter is $\{E_f \leq 0.01 \text{ eV/atom}, E_{abh} \leq 0.1 \text{ eV/atom}\}$. (4) **G filter**. To make sure the candidate structures are semiconductors, the band gaps should be positive values. As we all know, the PBE-based band gaps value of Materials project database are underestimated. To ensure every potential BMS candidate structures to be included, the structures with band gap greater than 0.01 eV are all passed to next filter. (5) **D filter**. Due to the special electronic structure of BMS, the magnetic moment will increase or decrease at the same time when it is doped with electrons or holes. Therefore, we use it as an important filter to screen BMS materials. In this work, the candidate structures are doped by 0.1 electron and 0.1 hole to

calculate its magnetic moment.

According to the statistic chart of the number of candidate structures in primary screening stages (see in lower-left panel of Figure 1), it can be found that the number of candidate structures are quickly reduced to acceptable number, specifically speaking, 781 compounds. Assuming that the data quality of Materials Project is perfect, all 781 compounds should be BMS materials. However, according to our test, it shows that some of the magnetic ground state of compounds are wrongly predicted, especially those compounds with Co elements, which unusually has two spin states: high spin and low spin.³¹ For example, the total energy and magnetic moment of entry mp-1174644 ($\text{Li}_4\text{MnCo}_2\text{O}_7$) in MP database is -5.8252 eV/atom and $11.0 \mu_B$, respectively. However, our further calculation shows that the Co of this system should be high spin. The real total energy and magnetic moment should be -5.8466 eV/atom and $12.0 \mu_B$, respectively. This validated results indicate that our screening in this work may miss some BMS candidate materials in MP database, which cannot be solved before the MP database is updated. At the same time, we cannot guarantee all of 781 candidate structures are technically BMS materials. To tackle this problem, we further use the secondary descriptors to refine our results.

From the lower-right panel of Figure 1, it can be found that there are three steps for the secondary descriptors. **Magnetic Order:** the magnetic ground state of 781 candidate structures are carefully investigated to search for those structures with FM order. To be specific, firstly, the FM order of all candidates are calculated to find the magnetic atom and corresponding energy E_{FM} . Then the antiferromagnetic (AFM) orders are set according to the number of magnetic

atoms. Theoretically, the magnetic ground state calculation is a tedious task that needs to consider all combinations of magnetic order and symmetry of structure.³² To simplify the calculation, we use the following scheme. Specifically, if the number of magnetic atoms equals 2, 3, 4, 5 and 6, the number of AFM orders are 1, 2, 3, $\frac{C_5^2}{2}$ and $\frac{C_6^3}{2}$, respectively. The corresponding energies are labeled as $E_{\{AFM\}-U}$. If the number magnetic atoms equals 1 or is larger than 6, then we build three types of supercell ($2 \times 1 \times 1$, $1 \times 2 \times 1$ and $1 \times 1 \times 2$) to decide the magnetic ground state, where the FM order is applied for unitcell and AFM order is used between unitcells. The corresponding energies are labeled as $E_{\{AFM\}-S}$. Besides, considering the high spin and low spin of Co element, all of structures with Co element adopt $1.3 \mu_B$ and $5.5 \mu_B$ as initial magnetic moment, which can be assigned by label "MAGMON" in the VASP input file. According to energy difference between E_{FM} and $E_{\{AFM\}-U}$ (or $E_{\{AFM\}-S}/2$), the magnetic ground state is then decided. **Exchange Energy:** The Curie temperature is closely related to magnetic exchange energy (E_{ex}). According to the above label, the E_{ex} is defined as: $E_{ex} = \max(E_{\{AFM\}-S}/2 - E_{FM})$ or $E_{ex} = \max(E_{\{AFM\}-U} - E_{FM})$. **Band Gap:** According to the refined magnetic ground state, the band gap of selected structures are recalculated by HSE06 functional to identify those structures with positive band gap and BMS feature.

Based on the screening scheme as described in Figure 1, we finally obtain 11 candidate BMS materials for spintronics, among which 1 structure (CoPtF₆, MP-ID: mp-556492, ICSD: 37447) is experimentally synthesized and 10 structures are theoretically predicted. Properties of obtained BMS materials are listed in Table 1, which is sorted by the exchange energy per magnetic atom. According to the statistic, the number of entries for V-, Cr-, Mn-, Fe-, Co- and Ni-based BMS are

1, 1, 2, 3, 3 and 1, respectively. Although 10 of 11 candidate BMS candidates are theoretically predicted structures, all of them have negative E_f and zero or small positive E_{abh} , which indicates that these structures may be synthesized by experiments in future. It is worth noting that the E_{ex} of mp-771246 is larger than 100 meV/atom, indicating it may have a high Curie temperature and be promising in spintronics application. For the rest structures, all of E_{ex} are less than 100 meV/atom and show a general tendency: the larger magnetic atom distance is, the smaller E_{ex} is. In order to have a clear understanding, we present the crystal structure of first 8 materials (The structures of left BMSs are supplied in the SI Figure S1) in Figure 2 due to their relatively large E_{ex} . It can be found that, all of structures have high symmetry and most of the unit cell of structures have at least 2 magnetic atoms.

In addition, according to our screening results, the energy of FM state and AFM are nearly degenerate for 6 entries, including $\text{Co}(\text{HO})_2$ (mp-24105), $\text{CaMg}_{14}\text{CoO}_{16}$ (mp-1036443), $\text{Dy}_2\text{CoTe}_2(\text{SO}_7)_2$ (mp-1190177), $\text{MnH}_8(\text{NF}_3)_2$ (mp-759690), K_2MnF_6 (mp-560127) and $\text{Li}_4\text{NiSn}_3(\text{PO}_4)_4$ (mp-776070) (See SI Table S1). Previous study shows that strain or doping can be an effective way to tune AFM state to FM state.¹⁷ As a test case, we use 2% strain for mp-759690($\text{MnH}_8(\text{NF}_3)_2$) to check its strain response. The results show that the ground state magnetic order of $\text{MnH}_8(\text{NF}_3)_2$ under this small strain is FM state and also present BMS feature (The corresponding DOS is supplied in the SI Figure S2).

Then the basic electronic structure properties of obtained BMSs are investigated. In Figure 3 we plotted the DOS for first 8 structures by using HSE06-based first-principles calculations (The

corresponding HSE06-based DOS for left entries are supplied in the SI Figure S3). We can find that all of 8 compounds possess completely spin polarized DOS with opposite spin orientations around the Fermi level. Due to the unique electronic structure, the spin direction of these BMS systems can be easily tuned by the electrical gating technique. A positive/negative gate voltage will inject electrons/holes into the BMS system, which causes a controllable half-metallic conducting behaviour.¹⁰

To estimate the Curie temperatures of obtained BMS materials, three methods are available, including mean-field approximation (MFA), random-phase approximation (RPA) and Monte Carlo simulation (MC).³³ Compared with RPA and MC, MFA usually overestimates the Curie temperature. In this work, we use MC method based on the classical Heisenberg Hamiltonian to estimate the Curie temperature:

$$H = - \sum_{i,j} J_{i,j} S_i S_j \quad (2)$$

where $J_{i,j}$ is the exchange parameter and S is the spin of magnetic atoms. Here, we consider two exchange parameters J_1 and J_2 (Labeled in Figure 4(a)), which represent the intralayer and interlayer nearest-neighbor exchange parameter respectively. The spin density of FM and AFM states are shown in Figure 4(a)-(c), where the local magnetic moments are all contributed by V atoms. For MC simulation, the supercell for $\text{Li}_2\text{V}_3\text{TeO}_8$ is set to be $8 \times 8 \times 8$. According to the E_{ex} in Table 1, we deduce that the $J_{i,j}$ of $\text{Li}_2\text{V}_3\text{TeO}_8$ is 33.3 meV and 15.7 meV. Then the simulated spin magnetic moment and susceptibility as a function of temperature are plotted in Figure 4(d). For $\text{Li}_2\text{V}_3\text{TeO}_8$, all the spins of V atoms point in the same direction at 0K, forming a strict FM order, while the magnetic moment decreases rapidly when heated. The critical point

for FM to paramagnetic transition occurs at about 478 K, as indicated by an abrupt increase in the magnetic susceptibility curve.

As discussed above, the bulk $\text{Li}_2\text{V}_3\text{TeO}_8$ is predicted to be a potential candidate for BMS. However, to design modern nano-sized devices, a thin film (slab) structure is required. Due to the surface states and quantum-size effect, the properties of two-dimensional (2D) slab structures are generally different from their bulk counterpart and depend on the slab's thickness. Therefore, it is necessary to answer the following questions: Can the 2D slab of $\text{Li}_2\text{V}_3\text{TeO}_8$ maintain the BMS feature? What is the smallest thickness required for maintaining stable BMS feature? For simplicity, we here only consider the (001) oriented slabs. According to the symmetry of $\text{Li}_2\text{V}_3\text{TeO}_8$, 5 slabs with different surface terminations are selected, namely, O1-, O2-, Te-, V- and Li-termination (See Figure S4). The calculation shows that the O1-termination has the lowest formation energy. Then the electronic properties of O1-termination with different number of V atom layers are tested. Considering that FM order will finally be the ground state as the number of V atom layers increases, here we only calculate the DOS of O1-terminated slabs with FM order to reduce the workload. According to DOS in Figure S5, it can be found that as the number of V atom layers increases, the electronic structure gradually converges. Specifically, when the number of V atom layers is greater than or equal to 6, the total magnetic moment will increase by $5 \mu_B$ for each additional V atom layer. At the same time, when the number of V atom layers reaches to 11, the slab structure shows BMS feature and the structure with 12 V atom layers also has the same feature and a similar DOS. That is to say, a minimum number of 11 V atom layers (corresponding to 5.34 nm) are required for spintronics application. The detailed properties of 2D $\text{Li}_2\text{V}_3\text{TeO}_8$

slabs with different thicknesses are summarized in Table S2.

Despite its potential application in spintronics devices design, the $\text{Li}_2\text{V}_3\text{TeO}_8$ is still not synthesized yet. However, according to the query results from MP database (see Table S3), it can be found that the formation energy and energy above hull are all lower than that of experimental phases LiVTeO_5 (ICSD: 21012) and $\text{LiV}_3(\text{TeO}_6)_2$ (ICSD: 249325) when the stable phases LiTe_3 (ICSD: 935), VTe_2 (ICSD: 38369) and TeO_2 (ICSD: 26844 and 30222) are selected as references. At the same time, the theoretically proposed reaction of $2\text{LiTe}_3 + 3\text{VTe}_2 + 15\text{O}_2 \rightarrow 11\text{TeO}_2 + \text{Li}_2\text{V}_3\text{TeO}_8$ has the largest reaction enthalpy change (exothermic reaction) compared with LiVTeO_5 and $\text{LiV}_3(\text{TeO}_6)_2$. Therefore, $\text{Li}_2\text{V}_3\text{TeO}_8$ would have possibility to be synthesized experimentally.

Discussion

In summary, based on initialization filter, magnetic filter, stability filter, band gap filter, doping filter and refinement filters, we propose a standard high-throughput computational screening scheme for exploring an important class of ferromagnetic semiconductors with electrically controllable spin polarization, namely BMS. Compared with the traditional trial and error method, the present scheme is direct and efficient. By using present scheme, a total number of 11 BMS materials are obtained via screening a comprehensive quantum materials repository containing 44703 magnetic compounds. Among them, $\text{Li}_2\text{V}_3\text{TeO}_8$ is predicted to be a room temperature BMS with a Curie temperature about 478 K. Meanwhile, the corresponding slab structure of $\text{Li}_2\text{V}_3\text{TeO}_8$ with 11 or

more V atom layers can maintain the bulk's BMS feature well. Besides, the low formation energy and energy above convex hull make the experimental synthesis of $\text{Li}_2\text{V}_3\text{TeO}_8$ feasible.

However, some drawbacks also exist for current scheme. For example, the DFT calculation is very expensive, which limits us to search for BMS materials with larger unitcell. In addition, the current MP database is not adequately qualified, which will result in the missing of some potential BMS candidates. To solve these problems, highly qualified database is needed. At the same time, based on existing BMS materials to build structure-properties relationship, then use machine learning method to predict new BMS is a feasible way. We will leave these problems in our future work and also wish our current work can guide experiments and theories for developing BMS materials.

Methods

The first-principles calculations of electronic structure are conducted by using the Vienna ab initio simulation package (VASP) software package.^{34,35} The generalized gradient approximation (GGA) of Perdew, Burke, and Ernzerhof (PBE) exchange correlation functional³⁶ with collinear spin polarization is employed. The plane wave basis set is used to describe the valence electrons with the cutoff set to 520 eV. The convergence criteria for electronic SCF iterations and ionic step iterations were set to be 1.0×10^{-6} eV and 0.5×10^{-3} eV \AA^{-1} , respectively. The reciprocal space grid was set to 8000 according to Pymatgen method.²⁸ To better describe onsite Coulomb repulsion among d or f electrons, we adopt the GGA+U scheme³⁷ during the screening stage, where the effective onsite coulomb interaction parameter (U) and exchange interaction parameter

(*J*) for different structures are set according to Pymatgen default values. To fix semi-local PBE calculations of electronic structures, the density of states (DOS) of final candidate materials are calculated based on screened hybrid HSE06 functional^{38,39} with 20% Hartree-Fock exchange.

In order to ensure that the large scale BMS screening tasks running on the HPC cluster in an efficient, stable, and automated manner, we use dpdispatcher (see in Code Availability) to create, manage and collect tasks. To generate input files of static and density of states calculation and to analyse output files, Pymatgen and mapprool (see in Code Availability) are used. The visualization of crystal structure is implemented by VESTA software.⁴⁰

Acknowledgements

Author Contributions Haidi Wang, XingXing Li and Jinlong Yang conceived the idea. Haidi Wang and Qingqing Feng performed the calculations. All authors helped to write, modify and analyze this manuscript.

Funding This work is financially supported by the Fundamental Research Funds for the Central Universities, by the National Natural Science Foundation of China (Grant No. 21688102), by the National Key Research & Development Program of China (Grant No. 2016YFA0200604), by Anhui Initiative in Quantum Information Technologies (Grant No. AHY090400), by the Youth Innovation Promotion Association CAS (2019441), and by USTC Research Funds of the Double First-Class Initiative (YD2060002011). The authors thank the Supercomputer platform of USTC, Beijing and HFUT for the computational resources.

Conflicts of Interest The authors declare that there are no competing interests.

Data Availability The authors confirm that the data supporting the findings of this study are available

within the article and its supplementary materials. All of the structures and related information can be downloaded online (<https://gitee.com/haidi-hfut/bms>).

Code Availability The dpdispatcher can be found at (<https://github.com/deepmodeling/dpdispatcher>). The maptool can be found at (<https://github.com/haidi-ustc/maptool>).

Supplementary Materials

Table for properties of entries mp-24105, mp-1036443, mp-1190177, mp-759690, mp-560127 and mp-776070; Crystal structure and density of state for $\text{Li}_4\text{Ni}_7(\text{OF}_7)_2$ (mp-867641), CoPtF_6 (mp-556492) and Li_2MnF_6 (mp-754966); density of state for $\text{MnH}_8(\text{NF}_3)_2$ under strain; density of state for $\text{Li}_4\text{Ni}_7(\text{OF}_7)_2$ (mp-867641), CoPtF_6 (mp-556492) and Li_2MnF_6 (mp-754966); table for properties of $\text{Li}_2\text{V}_3\text{TeO}_8$ of (001) oriented O1-termination slabs with different number of V atom layers; (001) oriented slabs of $\text{Li}_2\text{V}_3\text{TeO}_8$ with different surface terminations; density of state of $\text{Li}_2\text{V}_3\text{TeO}_8$ of (001) oriented O1-termination slabs; table for properties of Li-V-Te-O quaternary compounds $\text{Li}_2\text{V}_3\text{TeO}_8$, LiVTeO_5 and $\text{LiV}_3(\text{TeO}_6)_2$.

References

1. Fert, A. Nobel lecture: Origin, development, and future of spintronics nobel lecture: Origin, development, and future of spintronics. *Rev. Mod. Phys.* **80**, 1517–1530 (2008).
2. Dieny, B. *et al.* Opportunities and challenges for spintronics in the microelectronics industry. *Nat. Electron.* **3**, 446–459 (2020).
3. Wolf, S. A. *et al.* Spintronics: A spin-based electronics vision for the future. *Science* **294**, 1488–1495 (2001).

4. Hirohata, A. *et al.* Review on spintronics: Principles and device applications. *J. Magn. Magn. Mater.* **509**, 166711 (2020).
5. Ohno, Y. *et al.* Electrical spin injection in a ferromagnetic semiconductor heterostructure. *Nature* **402**, 790–792 (1999).
6. Li, X., Li, X. & Yang, J. Room-Temperature Ferromagnetism in Transition Metal Embedded Borophene Nanosheets. *J. Phys. Chem. Lett.* **10**, 4417–4421 (2019).
7. Gao, G. *et al.* Monolayer MXenes: promising half-metals and spin gapless semiconductors. *Nanoscale* **8**, 8986–8994 (2016).
8. Kan, M., Zhou, J., Sun, Q., Kawazoe, Y. & Jena, P. The Intrinsic Ferromagnetism in a MnO_2 Monolayer. *J. Phys. Chem. Lett.* **4**, 3382–3386 (2013).
9. Zhou, J. & Sun, Q. Magnetism of Phthalocyanine-Based Organometallic Single Porous Sheet. *J. Am. Chem. Soc.* **133**, 15113–15119 (2011).
10. Li, X., Wu, X., Li, Z., Yang, J. & Hou, J. G. Bipolar magnetic semiconductors: A new class of spintronics materials. *Nanoscale* **4**, 5680–5685 (2012).
11. Khalifeh, M., Safaiee, R. & Golshan, M. Magnetic bipolarity and other electronic aspects of (4,4) silicon carbide nanotubes ((4,4)-sicut) decorated by light noble metals; (cu, ag). *Appl. Surf. Sci.* **540**, 148323 (2021).
12. Zhang, J., Li, X. & Yang, J. SiN-SiC nanofilm: A nano-functional ceramic with bipolar magnetic semiconducting character. *Appl. Phys. Lett.* **104**, 172403 (2014).
13. Zha, X.-H. *et al.* Bipolar magnetic semiconductors among intermediate states during the conversion from $Sc_2C(OH)_2$ to Sc_2CO_2 MXene. *Nanoscale* **10**, 8763–8771 (2018).
14. Li, X. & Yang, J. Bipolar magnetic materials for electrical manipulation of spin-polarization orientation. *Phys. Chem. Chem. Phys.* **15**, 15793–15801 (2013).
15. Zhang, J., Zhao, B., Ma, C. & Yang, Z. Bipolar ferromagnetic semiconductors and doping-tuned room-temperature half-metallicity in monolayer MoX_3 (X=Cl, Br, I): An HSE06 study. *Phys. Rev. B* **103** (2021).

16. Yuan, L., Li, Z. & Yang, J. Hydrogenated bilayer wurtzite SiC nanofilms: a two-dimensional bipolar magnetic semiconductor material. *Phys. Chem. Chem. Phys.* **15**, 497–503 (2013).
17. Li, X. & Yang, J. First-principles design of spintronics materials. *Natl. Sci. Rev.* **3**, 365–381 (2016).
18. Li, X. & Yang, J. $CrXTe_3$ (X=Si, Ge) nanosheets: two dimensional intrinsic ferromagnetic semiconductors. *J. Mater. Chem. C* **2**, 7071–7076 (2014).
19. Zhang, D. *et al.* Hydrogenations and electric field induced magnetic behaviors in armchair silicene nanoribbons. *Sci. Rep.* **6**, 23677 (2016).
20. Ding, Y. & Wang, Y. Intrinsic ferromagnetism and valley polarization in hydrogenated group V transition-metal dinitride (MN_2H_2 , M = V/Nb/Ta) nanosheets: insights from first-principles. *Nanoscale* **12**, 1002–1012 (2020).
21. Wang, B. *et al.* Prediction of a two-dimensional high-TC f-electron ferromagnetic semiconductor. *Mater. Horiz.* **7**, 1623–1630 (2020).
22. NIST. Material Genome Project (2011). URL <https://www.nist.gov/mgi>.
23. Jain, A. *et al.* Commentary: The Materials Project: A materials genome approach to accelerating materials innovation. *APL Mater.* **1**, 011002 (2013).
24. Urban, A., Matts, I., Abdellahi, A. & Ceder, G. Computational Design and Preparation of Cation-Disordered Oxides for High-Energy-Density Li-Ion Batteries. *Adv. Energy Mater.* **6**, 1600488 (2016).
25. Yan, Q. *et al.* Solar fuels photoanode materials discovery by integrating high-throughput theory and experiment. *Proc. Natl. Acad. Sci. U.S.A.* **114**, 3040–3043 (2017).
26. Chen, W., George, J., Varley, J. B., Rignanese, G.-M. & Hautier, G. High-throughput computational discovery of $In_2Mn_2O_7$ as a high Curie temperature ferromagnetic semiconductor for spintronics. *npj Comput. Mater.* **5**, 72 (2019).
27. Ong, S. P. *et al.* The materials application programming interface (API): A simple, flexible and efficient API for materials data based on REpresentational state transfer (REST) principles. *Comput. Mater. Sci* **97**, 209–215 (2015).

28. Ong, S. P. *et al.* Python Materials Genomics (pymatgen): A robust, open-source python library for materials analysis. *Comput. Mater. Sci* **68**, 314–319 (2013).
29. Wang, H., Zhang, Y., Zhang, L. & Wang, H. Crystal Structure Prediction of Binary Alloys via Deep Potential. *Front. Chem.* **8**, 1–9 (2020).
30. Haastrup, S. *et al.* The Computational 2D Materials Database: High-throughput modeling and discovery of atomically thin crystals. *2D Mater.* **5**, 042002 (2018).
31. Kremer, S., Henke, W. & Reinen, D. High-spin-low-spin equilibriums of cobalt(2+) in the terpyridine complexes $Co(terpy)_2X_2 \cdot nH_2O$. *Inorg. Chem.* **21**, 3013–3022 (1982).
32. Horton, M. K., Montoya, J. H., Liu, M. & Persson, K. A. High-throughput prediction of the ground-state collinear magnetic order of inorganic materials using Density Functional Theory. *npj Comput. Mater.* **5**, 64 (2019).
33. Ruzs, J., Bergqvist, L., Kudrnovský, J. & Turek, I. Exchange interactions and curie temperatures in $ni_{2-x}MnSb$ alloys: First-principles study. *Phys. Rev. B* **73**, 214412 (2006).
34. Kresse, G. & Furthmüller, J. Efficient iterative schemes for ab initio total-energy calculations using a plane-wave basis set. *Phys. Rev. B* **54**, 11169–11186 (1996).
35. Kresse, G. & Furthmüller, J. Efficiency of ab-initio total energy calculations for metals and semiconductors using a plane-wave basis set. *Comput. Mater. Sci* **6**, 15–50 (1996).
36. Perdew, J. P., Burke, K. & Ernzerhof, M. Generalized gradient approximation made simple. *Phys. Rev. Lett.* **77**, 3865 (1996).
37. Liechtenstein, A. I., Anisimov, V. I. & Zaanen, J. Density-functional theory and strong interactions: Orbital ordering in mott-hubbard insulators. *Phys. Rev. B* **52**, R5467–R5470 (1995).
38. Heyd, J., Scuseria, G. E. & Ernzerhof, M. Hybrid functionals based on a screened coulomb potential. *J. Chem. Phys.* **118**, 8207–8215 (2003).
39. Heyd, J., Scuseria, G. E. & Ernzerhof, M. Erratum: “Hybrid functionals based on a screened Coulomb potential” [J. Chem. Phys. 118, 8207 (2003)]. *J. Chem. Phys.* **124**, 219906 (2006).

40. Momma, K. & Izumi, F. VESTA: A three-dimensional visualization system for electronic and structural analysis. *J. Appl. Crystallogr.* **41**, 653–658 (2008).

Figures and Table

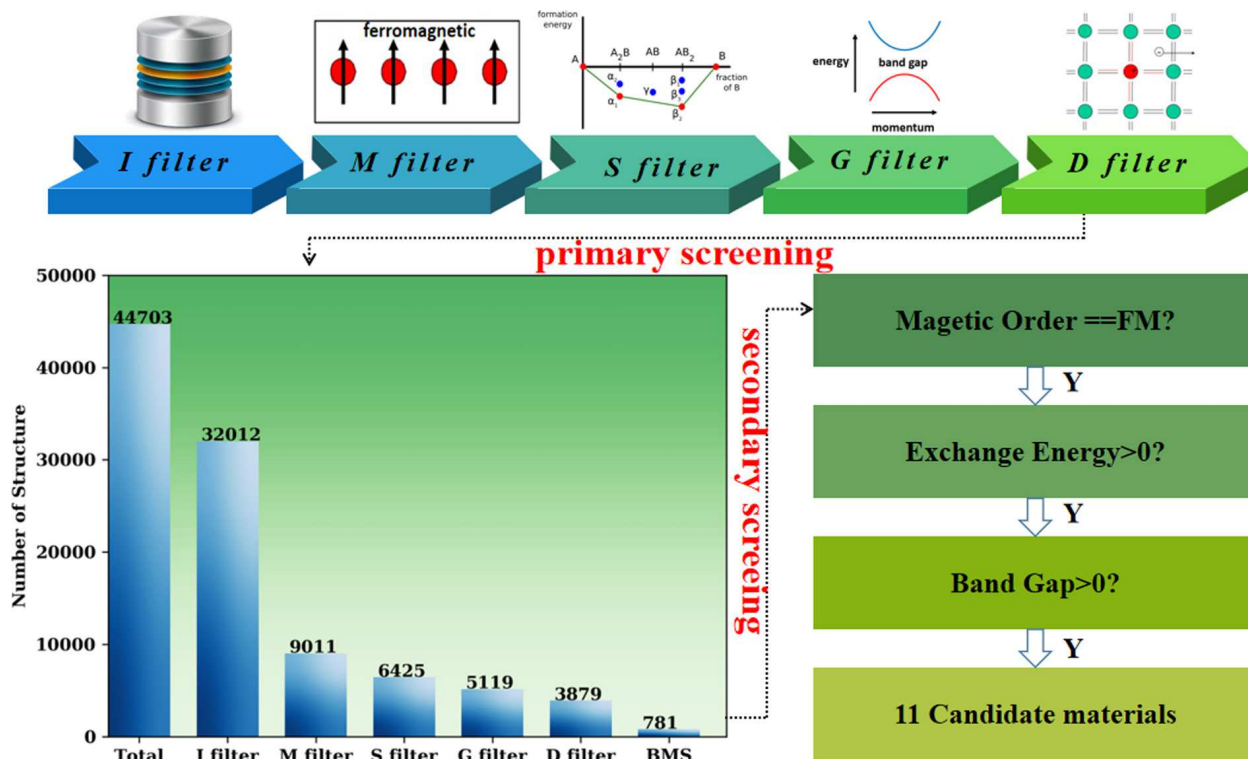


Figure 1: Up panel: schematic diagram of the primary descriptors for high-throughput screening process, including Initialization filter, magnetic filter, stability filter, band gap filter and doping filter. lower-left panel: Statistic chart of the number of candidate structures in different screening stages. lower-right panel: Secondary descriptors for BMS screening.

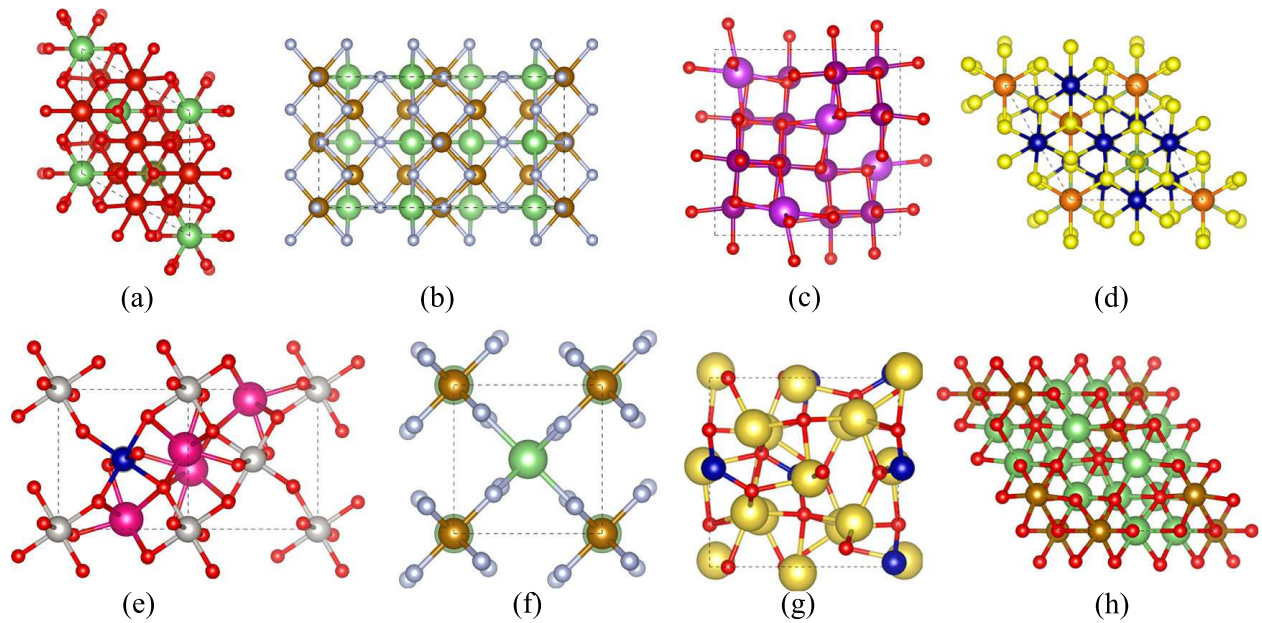


Figure 2: (a)-(h) Crystal structure of $\text{Li}_2\text{V}_3\text{TeO}_8$ (mp-771246), $\text{Li}_2\text{Fe}_3\text{F}_8$ (mp-1177989), Mn_3BiO_8 (mp-773037), $\text{Mg}_2\text{Cr}_3\text{GaS}_8$ (mp-1247148), $\text{Sm}_2\text{CoPtO}_6$ (mp-1208920), LiFeF_6 (mp-1222351), Na_3CoO_3 (mp-755811) and Li_3FeO_4 (mp-849528), respectively

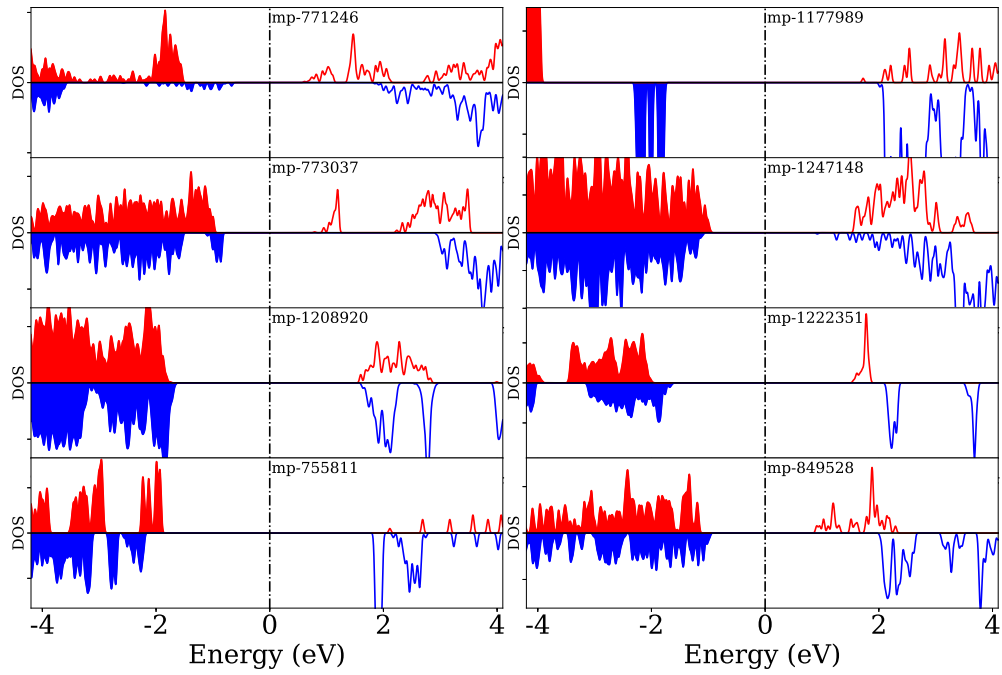


Figure 3: HSE06 level density of states for $\text{Li}_2\text{V}_3\text{TeO}_8$ (mp-771246), $\text{Li}_2\text{Fe}_3\text{F}_8$ (mp-1177989), Mn_3BiO_8 (mp-773037), $\text{Mg}_2\text{Cr}_3\text{GaS}_8$ (mp-1247148), $\text{Sm}_2\text{CoPtO}_6$ (mp-1208920), LiFeF_6 (mp-1222351), Na_3CoO_3 (mp-755811) and Li_3FeO_4 (mp-849528), respectively

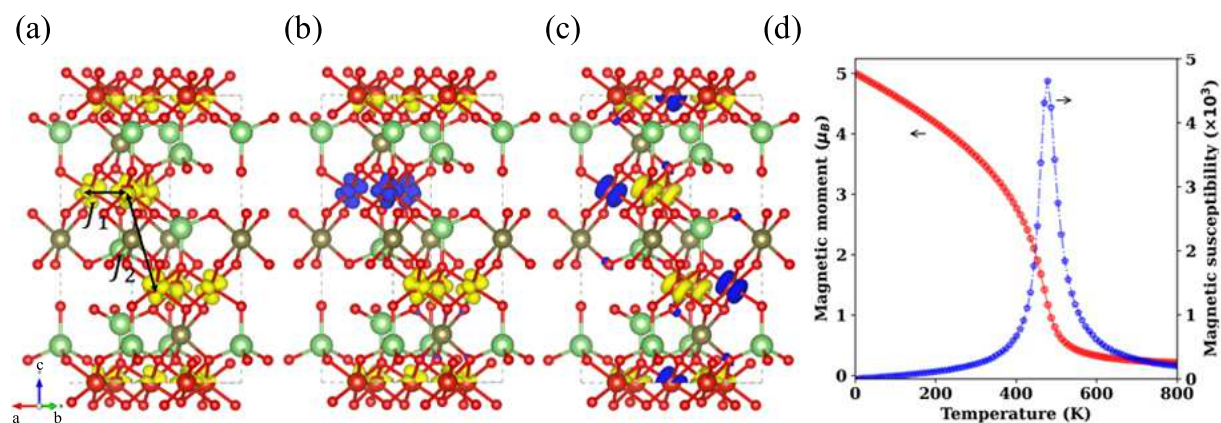


Figure 4: Isosurface of spin density of (a) ferromagnetic state and (b)-(c) antiferromagnetic state of $\text{Li}_2\text{V}_3\text{TeO}_8$ with an isovalue of $0.031 \text{ eV}/\text{\AA}^3$. Yellow and blue indicate the positive and negative values, respectively. (d) The evolution of spin magnetic moment (red circle) per unit cell and magnetic susceptibility (green pentagon) with respect to temperature for $\text{Li}_2\text{V}_3\text{TeO}_8$ (mp-771246).

Table 1: Properties of obtained compounds for BMS materials based PBE level simulation: Materials Project ID (MP-ID), formula, formation energy (E_f , eV/atom), energy above hull (E_{abh} , eV/atom), magnetic moment per formula unit cell (m , μ_B /f.u.), minimum distance between magnetic atoms (d_{min} , Å), number of magnetic atom (N_m), exchange energy per magnetic atom (E_{ex} , meV/atom) and space group symmetry. The spin-flip gap in valence band (Δ_1 , eV), conduction band (Δ_2 , eV) and the band gap (Δ_3 , eV)

MP-ID	formula	E_f	E_{abh}	m	d_{min}	N_m	E_{ex}	symmetry	Δ_1	Δ_2	Δ_3
mp-771246	Li ₂ V ₃ TeO ₈	-2.270	0.045	6	3.021	3	180	R-3m	0.855	1.259	0.254
mp-1177989	Li ₂ Fe ₃ F ₈	-2.863	0.034	13	3.168	6	71	Cmce	1.242	0.414	3.124
mp-773037	Mn ₃ BiO ₈	-1.673	0.060	8	2.898	12	49	$P4_332$	0.068	2.179	0.613
mp-1247148	Mg ₂ Cr ₃ GaS ₈	-1.252	0.041	9	3.622	3	21	R-3m	0.450	0.507	0.366
mp-1208920	Sm ₂ CoPtO ₆	-2.566	0.005	4	5.427	2	19	$P2_1/c$	0.127	0.025	1.627
mp-1222351	LiFeF ₆	-2.265	0.000	4	4.738	2	3	$P4_2nm$	0.121	1.365	1.124
mp-755811	Na ₃ CoO ₃	-1.562	0.038	5	5.101	4	3	$P2_13$	0.663	0.340	1.803
mp-849528	Li ₃ FeO ₄	-1.872	0.015	3	3.082	4	2	I-43m	0.115	1.769	0.231
mp-867641	Li ₄ Ni ₇ (OF ₇) ₂	-2.264	0.062	15	2.975	7	2	C2/m	0.440	0.308	2.815
mp-556492	CoPtF ₆	-1.997	0.000	4	5.192	1	2	R-3	0.040	0.020	1.841
mp-754966	Li ₂ MnF ₆	-2.888	0.000	4	4.667	2	1	$P4_2/mnm$	0.073	1.418	2.617

Supplementary Materials: High-throughput computational screening for bipolar magnetic semiconductors

Haidi Wang¹, Qingqing Feng², Xingxing Li^{2*} & Jinlong Yang^{2*}

¹*School of Physics, Hefei University of Technology, Hefei, Anhui 230601, China*

²*Hefei National Laboratory for Physical Sciences at Microscale, Department of Chemical Physics, and Synergetic Innovation Center of Quantum Information and Quantum Physics, University of Science and Technology of China, Hefei, Anhui 230026, China*

Correspondence Xingxing Li (lix@ustc.edu.cn) & Jinlong Yang (jlyang@ustc.edu.cn)

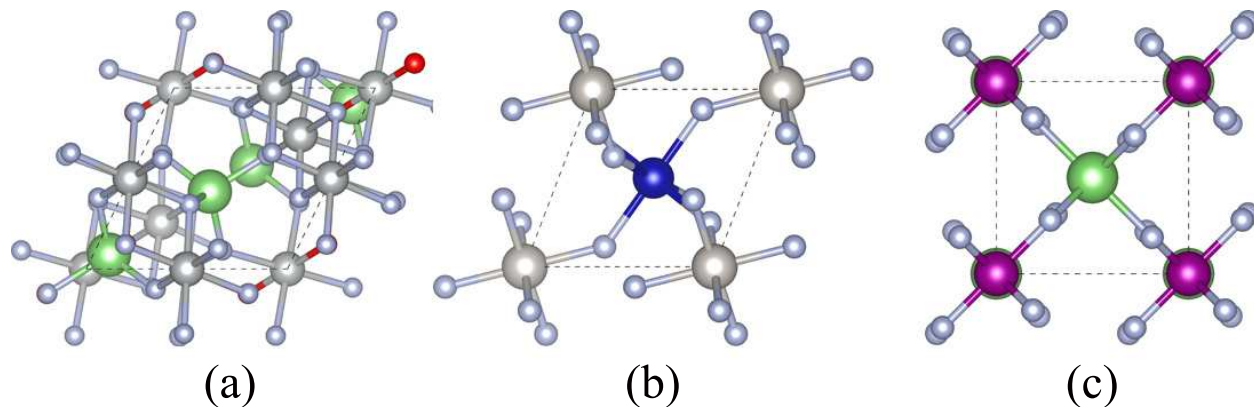


Figure S 1: (a)-(c) Crystal structure of $\text{Li}_4\text{Ni}_7(\text{OF}_7)_2$ (mp-867641), CoPtF_6 (mp-556492) and Li_2MnF_6 (mp-754966), respectively.

Table S 1: Properties of obtained compounds for BMS materials based PBE level simulation: Materials Project ID (MP-ID), formula, formation energy (E_f , eV/atom), energy above hull (E_{abh} , eV/atom), magnetic moment per formula unit cell (m , μ_B /f.u.), minimum distance between magnetic atoms (d_{min} , Å), number of magnetic atom (N_m), exchange energy per magnetic atom (E_{ex} , meV/atom) and space group symmetry. The spin-flip gap in valence band (Δ_1 , eV), conduction band (Δ_2 , eV) and the band gap (Δ_3 , eV)

MP-ID	formula	E_f	E_{abh}	m	d_{min}	N_m	E_{ex}	symmetry	Δ_1	Δ_2	Δ_3
mp-24105	Co(HO) ₂	-1.361	0.037	3.000	3.196	1	0.0084	P-3m1	0.282	0.199	2.288
mp-1036443	CaMg ₁₄ CoO ₁₆	-2.939	0.036	3.000	4.320	1	0.0054	Pmmm	0.367	0.818	2.087
mp-1190177	Dy ₂ CoTe ₂ (SO ₇) ₂	-2.426	0.000	3.000	5.301	1	0.0005	P-1	0.070	0.402	2.991
mp-759690	MnH ₈ (NF ₃) ₂	-1.611	0.089	3.000	5.876	2	0.0005	$P6_3mc$	0.069	1.335	3.114
mp-560127	K ₂ MnF ₆	-2.915	0.001	3.000	5.834	2	0.0004	$P6_3mc$	0.068	1.322	3.153
mp-776070	Li ₄ NiSn ₃ (PO ₄) ₄	-2.365	0.087	1.999	4.845	1	0.00003	Pm	0.082	0.247	2.306

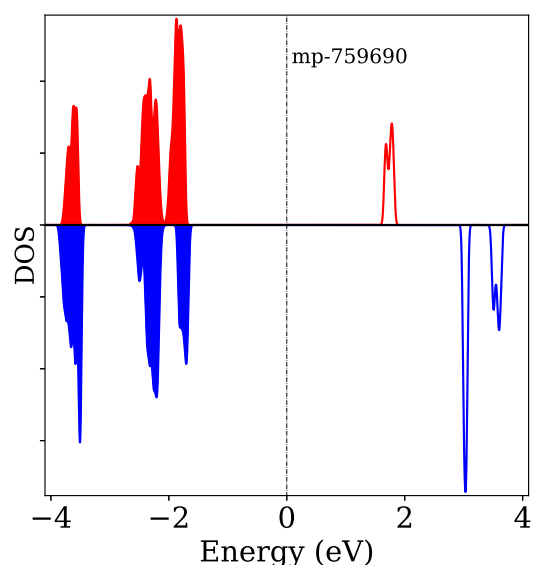


Figure S 2: Density of state for MnH₈(NF₃)₂ (mp-759690) with 2% strain under PBE level theory.

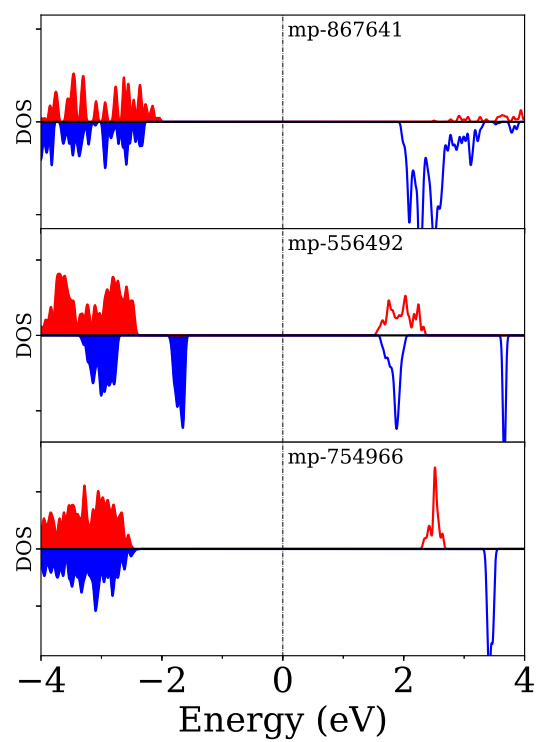


Figure S 3: Density of state for $\text{Li}_4\text{Ni}_7(\text{OF}_7)_2$ (mp-867641), CoPtF_6 (mp-556492) and Li_2MnF_6 (mp-754966), respectively.

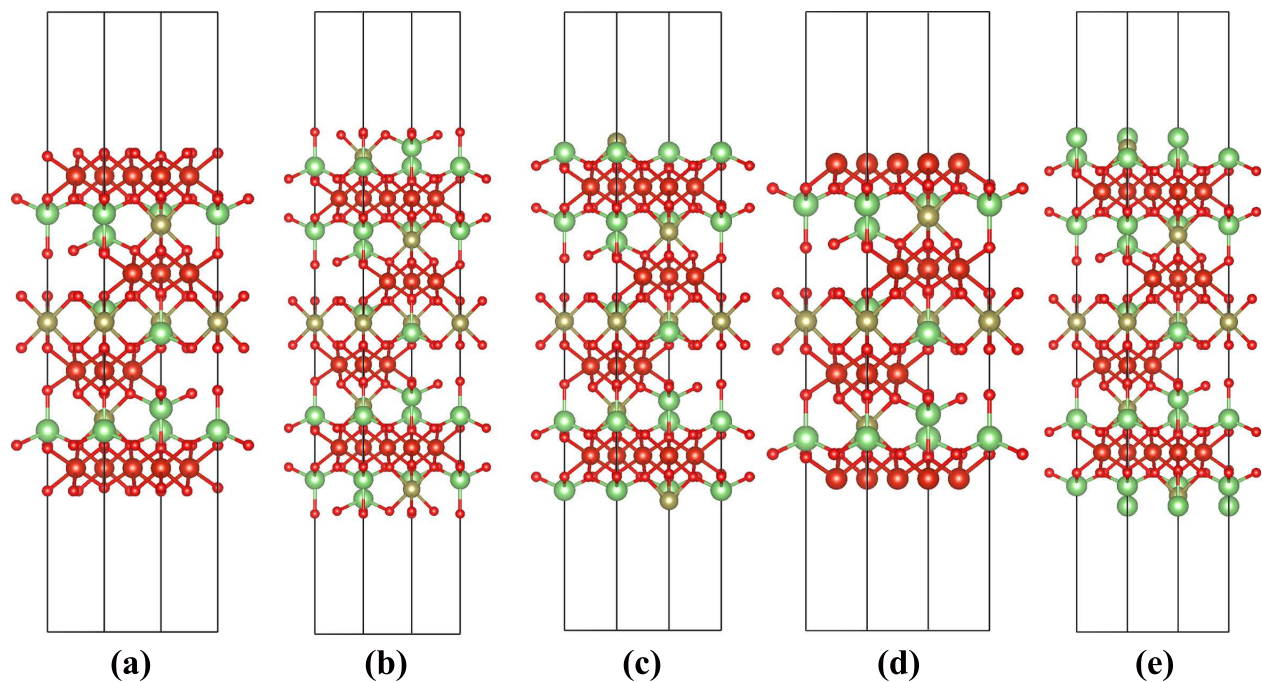


Figure S 4: (001) oriented slabs of $\text{Li}_2\text{V}_3\text{TeO}_8$ with different surface terminations. (a)-(e) are O1-, O2-, Te-, V- and Li-termination, respectively. The corresponding formation energies are -1.463 eV, -1.333 eV, -1.415 eV, -1.247 eV and -1.460 eV, respectively

Table S 2: Properties of $\text{Li}_2\text{V}_3\text{TeO}_8$ of (001) oriented O1-termination slabs with different number of V atom layers: layer numbers (n_{Layer}), number of total atoms (N_{atom}), formula, magnetic moment per unit cell ($m, \mu_B/\text{f.u.}$) and classification according to the band structure of spintronics materials. HM and HSC represent half metal and half semiconductor, respectively

n_{Layer}	N_{atom}	formula	m	classification
2	25	$\text{Li}_2\text{V}_6\text{TeO}_{16}$	6.00	HSC
3	39	$\text{Li}_4\text{V}_9\text{Te}_2\text{O}_{24}$	9.00	HM
4	53	$\text{Li}_6\text{V}_{12}\text{Te}_3\text{O}_{32}$	16.00	BMS
5	67	$\text{Li}_8\text{V}_{15}\text{Te}_4\text{O}_{40}$	19.00	HSC
6	81	$\text{Li}_{10}\text{V}_{18}\text{Te}_5\text{O}_{48}$	28.00	HM
7	95	$\text{Li}_{12}\text{V}_{21}\text{Te}_6\text{O}_{56}$	33.00	HM
8	109	$\text{Li}_{14}\text{V}_{24}\text{Te}_7\text{O}_{64}$	38.00	HM
9	123	$\text{Li}_{16}\text{V}_{27}\text{Te}_8\text{O}_{72}$	43.00	HM
10	137	$\text{Li}_{18}\text{V}_{30}\text{Te}_9\text{O}_{80}$	48.00	HM
11	151	$\text{Li}_{20}\text{V}_{33}\text{Te}_{10}\text{O}_{88}$	53.00	BMS
12	165	$\text{Li}_{22}\text{V}_{36}\text{Te}_{11}\text{O}_{96}$	58.00	BMS

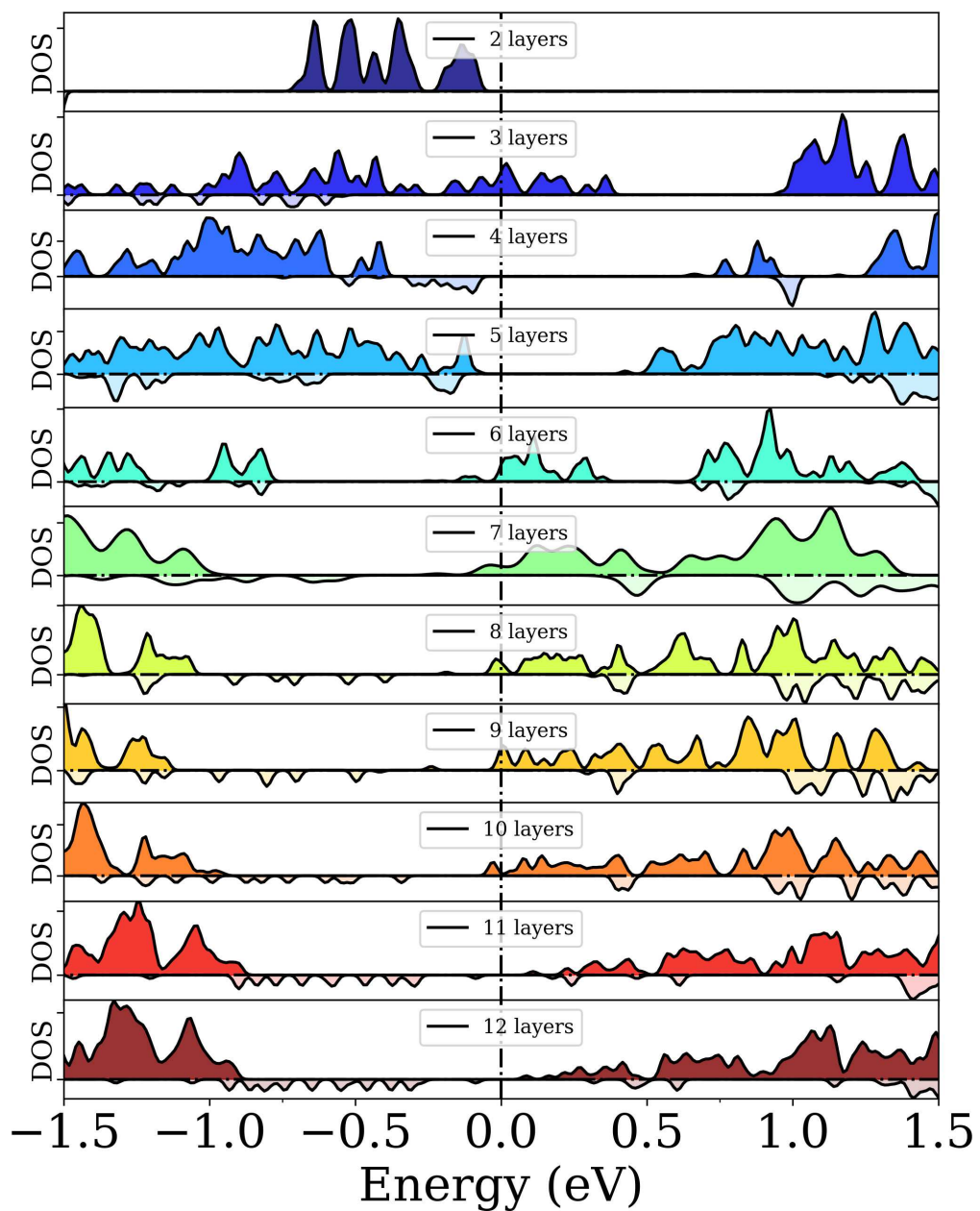


Figure S 5: Density of state of $\text{Li}_2\text{V}_3\text{TeO}_8$ of (001) oriented O1-termination slabs with number of V atom layer ranging from 2 to 12.

Table S 3: Properties of Li-V-Te-O quaternary compounds that queried from MP database: Materials Project ID (MP-ID), formula, formation energy (E_f , eV/atom), energy above hull (E_{abh} , eV/atom), reaction expression and reaction enthalpy change (kJ/mol). The reference systems are stable phases LiTe_3 , VTe_2 and TeO_2 .

MP-ID	formula	E_f	E_{abh}	Reaction	ΔH
mp-771246	$\text{Li}_2\text{V}_3\text{TeO}_8$	-0.248	0.03	$2\text{LiTe}_3 + 3\text{VTe}_2 + 15\text{O}_2 \rightarrow 11\text{TeO}_2 + \text{Li}_2\text{V}_3\text{TeO}_8$	-6798
mp-1181006	LiVTeO_5	-0.118	0.06	$2\text{LiTe}_3 + 2\text{VTe}_2 + 13\text{O}_2 \rightarrow 8\text{TeO}_2 + 2\text{LiVTeO}_5$	-5777
mp-559938	$\text{LiV}_3(\text{TeO}_6)_2$	-0.132	0.10	$\text{LiTe}_3 + 3\text{VTe}_2 + 13\text{O}_2 \rightarrow 7\text{TeO}_2 + \text{LiV}_3(\text{TeO}_6)_2$	-5821